Parameter Identification for Modeling Steel Fiber Reinforced Concrete under Compression to Prevent Concrete Cover Spalling under Severe Earthquake Loading Condition

Nia Dwi Puspitasari[1], *Bambang* Piscesa[1*], *Mario* M. Attard[2], *Dwi* Prasetya[1], *Faimun* Faimun[1], *Pujo* Aji[1], *Priyo* Suprobo[1]

[1]Civil Engineering Department, Institut Teknologi Sepuluh Nopember, 60111 Surabaya, Indonesia
[2]School of Civil and Environmental Engineering, University of New South Wales, NSW 2052, Sydney, Australia.

Abstract. The use of steel fiber in concrete material can improves both the strength and the ductility of concrete. The fibers can postpone or mitigate the concrete cover spalling under severe loading conditions such as during an earthquake. In this paper, the behavior of Steel Fiber Reinforced Concrete (SFRC) under compression is modeled using the Attard and Setunge's stress-strain model. The parameter identification consisted of the elastic modulus (E_c), the peak strength (f_{cc}), the residual strength (f_{res}), and the peak strain of concrete under compression (ε_{cc}). From the investigation, it is found that the models proposed for active confined concrete can be applied for steel fiber reinforced concrete. It was also shown that the axial strain at peak stress increases as the fiber volumetric ratio and fiber aspect ratio increased. A simple formula to predict the approximate value of confining pressure to account for the steel fiber presence is proposed. The verification of the proposed model with the experimental results is presented in detail. Furthermore, insight into the performance of the reinforced concrete column made of SFRC using the fiber-based cross-sectional analysis is sighted.

1 Introduction

During earthquakes, reinforced concrete members may experience significant lateral deformation accompanied by the concrete cover spalling due to large compressive strain [1]. Normal concrete has a relatively low tensile strength and for structural applications it is normal practice to incorporate steel bars to withstand tensile forces. The tensile strength of concrete can be estimated to be approximately between 9-15% of its compressive strength. To improve its performance and prevent the cover spalling, the use of steel fiber is found to be promising [2-4]. As a composite material, the steel fiber acts as a bridge to postpone the propagation of cracks and improve several characteristics and properties of the concrete.

With the presence of steel fiber, the peak axial strength and the axial strain at peak stress for concrete are enhanced which is as if a small active confining pressure were applied to the concrete. Furthermore, as the concrete with steel fiber is loaded beyond the peak strength, the concrete shows some residual strength capacity. This enhancement is found to be affected by the fiber volumetric ratio. However, the elastic modulus of the concrete is decreased as the fiber volumetric ratio increases [5].

This paper presents the parameter identification for modeling the Steel-Fiber Reinforced Concrete (SFRC) under compression to prevent concrete cover spalling under excessive axial strain exposed on the column. The empirically based stress-strain model proposed by Attard and Setunge [6] is used. The parameters being identified are the axial peak stress, the axial peak strain at peak stress, and the axial residual strength of concrete as a function of the fiber properties and fiber contents in the concrete. To further investigate the effect of steel fiber on the RC column, numerical simulation using the fiber-based nonlinear sectional analysis in MatLab is used.

2 Typical Response of Concrete with and without Steel Fiber

Fig. 1 shows the typical response of the axial stress and axial strain of plain concrete and SFRC loaded under uniaxial compression. Both the plain concrete and SFRC axial stress-strain curve consisted of two distinct branches which are the ascending and descending branches. As shown in Fig. 1, the axial peak stress of SFRC is higher than that of plain concrete. Similar behavior of the axial strain at peak stress of SFRC is also higher than the that of plain concrete. For SFRC, the steel fiber, at some stage, can restrain crack propagation in the concrete when the concrete softens which results in the presence of residual strength (f_{res}) in SFRC. For plain concrete loaded under compression when the concrete is crushed, the residual strength performance is smaller than SFRC. This can be

* Corresponding author: piscesa@ce.its.ac.id

understood because there is no mechanism that restrains the shear diagonal crack in the concrete.

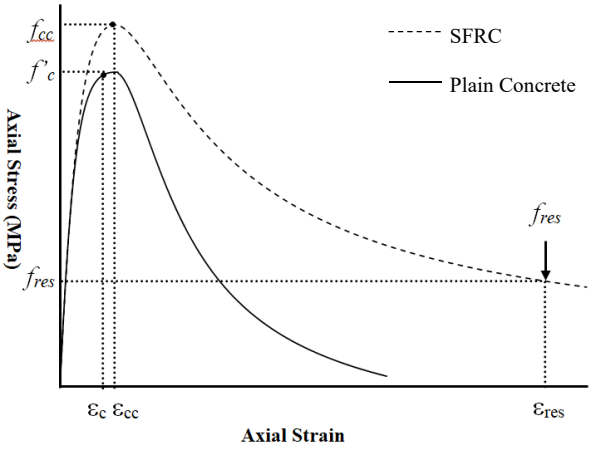

Fig. 1 Typical stress-strain relationship for SFRC and plain concrete

In Fig. 1, the stress-response of SFRC is similar to that of actively confined concrete. Hence, it is possible to predict the behavior of SFRC using the concrete constitutive model for concrete under active confinement. The material properties enhancement can be simply related to the artificial confining pressure provided by the steel fiber.

3 Parameter Identification

In order to identify the parameter that should be adjusted when the actively confined concrete model is used to predict the response of SFRC, available experimental test in the literature are gathered. From the available data, the axial peak stress and axial strain at peak stress can be easily identified. Hence, the SFRC tested specimen and the existing confined concrete model can be carried out by simply rearranging the peak stress formulation for actively confined concrete. In [6], the peak stress formulation can be defined as:

$$\frac{f_{cc}}{f_c^{'}} = \left(\frac{f_r}{f_t} + 1\right)^k \tag{1}$$

In the above, f_r is the confining pressure, f_{cc} is the axial peak stress, f_t is concrete uniaxial tensile strength, and the expression for k is:

$$k = 1.25\left[1 + 0.062\frac{f_r}{f_c^{'}}\right]\left(f_c^{'}\right)^{-0.21} \tag{2}$$

The value of f_r from Eq. (1) cannot be obtained directly. Hence, a root-finding method such as Secant-Method is used to get f_r for a given value for f_{cc} from the SFRC tested specimen.

Once the confining pressure is obtained, the predicted axial strain at peak stress (ε_{cc}) can be computed by [6]:

$$\frac{\varepsilon_{cc}}{\varepsilon_{cu}} = 1 + \left(17 - 0.06 f_c^{'}\right)\left(\frac{f_r}{f_c^{'}}\right) \tag{3}$$

In the above equation, ε_{cu} is the uniaxial axial strain at peak stress. It should be noted that the values for f'_c and ε_{cu} are obtained from the experimental data as shown in Table 1, where the f'_c is the compressive strength of plain concrete. From the gathered axial stress versus the axial strain data, it was difficult to set the point for the residual stresses. Therefore, to evaluate the Attard and Setunge [6] formulation (shown in Eq. 1 in this paper) in predicting the softening behavior of SFRC concrete, only the data with axial stress lower than eighty percent of the axial stress at peak stress is investigated. Checking the softening curve is carried out at the end of the stress-strain curve. Table 1 shows the data used in this paper. The data was gathered from the available experimental test in the literature [9-15].

Fig. 2 shows the residual strength comparison between the experimental test and prediction using the Attard and Setunge concrete constitutive model [6]. As shown in Fig. 2, the data was scattered around the 45-degree line. These phenomena show that for a low to medium confinement, the residual strength of SFRC concrete varies which is similar to the gathered test for actively confined concrete [7, 8]. However, as the confining pressure increases, data accuracy increases.

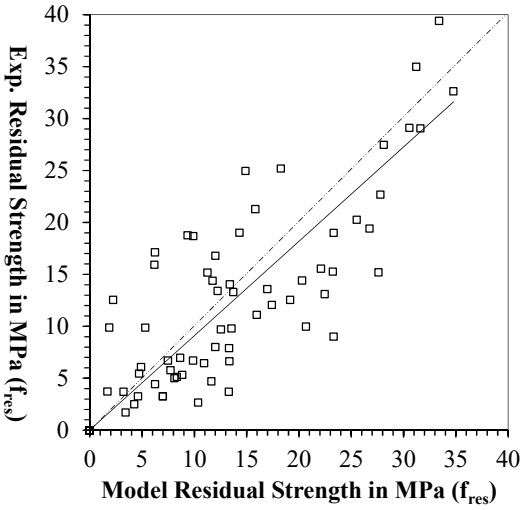

Fig. 2 Comparison between the residual stress (f_{res}) from the test result and the Attard and Setunge model [6]

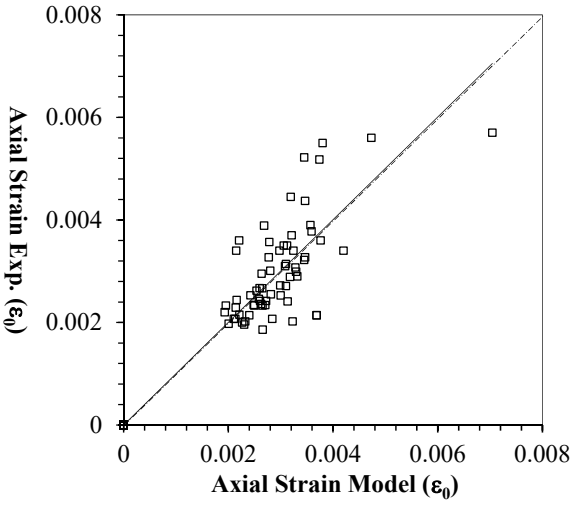

Fig. 3 Comparison of the axial strain at peak stress between the available experimental data and the Attard and Setunge model [6]

Table 1 Summary of experimental data from previous researchers

Researchers	Specimen ID	f_c' (MPa)	ε_c	f_{cc} (MPa)	ε_{cc}	V_f (%)	$\frac{l}{d}$	f_{ut} (MPa)
Dhakal, et al. [9]	P1	33.20	0.00360	33.20	0.00360	0.00	64	1100
	P4	25.50	0.00300	30.70	0.00360	0.50		
	P2	27.00	0.00380	29.70	0.00560	1.00		
	P3	28.70	0.00320	30.80	0.00360	1.00	43	1150
	P5	28.80	0.00330	41.20	0.00570	1.50		
	P6	25.60	0.00270	31.10	0.00340	2.00		
Błaszczyński and Przybylska-Fałek [10]	BZ1	35.58	0.00197	37.50	0.00215	0.50	50	-
	BZ3			42.00	0.00255	3.00		
Neves and De Almeida [11]	A.30.Z	38.30	0.00194	36.50	0.00195	0.38	55	1150
	A.30.R			40.00	0.00207		80	2300
	A.60.Z			33.30	0.00201	0.75	55	1150
	A.60.R			40.10	0.00229		80	2300
	A.90.Z			33.70	0.00214	1.13	55	1150
	A.90.R			44.40	0.00233		80	2300
	A.120.Z			30.70	0.00216	1.50	55	1150
	B.30.Z	62.20	0.00238	62.10	0.00235	0.38	55	1150
	B.30.R			65.30	0.00242		80	2300
	B.60.Z			65.00	0.00246	0.75	55	1150
	B.60.R			62.80	0.00253		80	2300
	B.90.Z			58.50	0.00254	1.13	55	1150
	B.90.R			65.70	0.00295		80	2300
	B.120.R			67.90	0.00301	1.50	80	2300
Marara, et al. [12]	N-60-0.5	32.06	0.00202	32.66	0.00207	0.50	60	-
	N-60-1			34.11	0.00202	1.00		
	N-60-1.25			36.28	0.00186	1.25		
	N-60-1.5			37.46	0.00207	1.50		
	N-60-1.75			39.27	0.00241	1.75		
	N-60-2			39.85	0.00202	2.00		
	N-75-0.5			33.73	0.00200	0.50	75	
	N-75-1			34.63	0.00214	1.00		
	N-75-1.25			36.61	0.00234	1.25		
	N-75-1.5			38.31	0.00340	1.50		
	N-75-1.75			39.63	0.00445	1.75		
	N-75-2			41.17	0.00522	2.00		
	N-83-0.5			33.99	0.00196	0.50	83	
	N-83-1			35.26	0.00233	1.00		
	N-83-1.25			37.09	0.00357	1.25		
	N-83-1.5			39.73	0.00370	1.50		
	N-83-1.75			41.27	0.00437	1.75		
	N-83-2			42.87	0.00518	2.00		

Researchers	Specimen ID	f_c' (MPa)	ε_c	f_{cc} (MPa)	ε_{cc}	V_f (%)	$\frac{l}{d}$	f_{ut} (MPa)
Nataraja, et al. [13]	M9	43.01	0.0027	45.84	0.00310	0.50	64	1100
	M10			41.59	0.00330	0.75		
	M11			46.97	0.00340	1.00		
	M12			45.65	0.00350	0.50	43	1150
	M13			46.12	0.00350	0.75		
	M14			49.23	0.00390	1.00		
Soroushian and Bayasi [14]	SR-57	41.86	0.00185	43.00	0.00233	2.00	57	-
	Cro			45.10	0.00244			
	Cre			43.54	0.00197			
	HC-60			45.60	0.00360		60	
	HS			50.12	0.00389			
	SR-72			42.00	0.00220		72	
	HC-75			44.16	0.00340			
Fanella and Naaman [15]	100-2	58.65	0.00337	62.44	0.00550	2.00	100	620 - 829
	83-2			60,97	0.00477	2.00	83	
	47-2			58,02	0.00383	2.00	47	
	83-1	60.72	0.00339	61.41	0.00214	1.00	83	

ε_c = strain at compressive strength; V_f = fiber volume fraction; $\frac{l}{d}$ = fiber aspect ratio

Fig. 3 shows the comparison between the axial strain at peak stress from the available experimental data and the Attard and Setunge model [6]. As shown in Fig. 3, most prediction for the axial strain at peak stress using the Attard and Setunge model [6] is excellent.

4 Comparison between Attard and Setunge Model and Available Experimental Test of Plain SFRC under Compression

In this section, a comparison between the available experimental test of plain SFRC under compression and the Attard and Setunge model [6] is presented. It should be noted that the parameter used in the model was obtained using the parameter identification method in section 3. Thus, it can later be seen that the peak stress between the experimental test and the model is exactly equal. Four specimens from four different researchers are selected.

Fig. 4 shows the comparisons between the stress-strain relationship from the selected experimental test and the Attard and Setunge model [6]. A comparison of the model with specimen B60R tested by Neves and De Almeida [11] shows an excellent agreement for both the ascending and descending branches of the stress-strain curve. Comparison with specimen M12 tested by Nataraja, et al. [13] shows excellent prediction for the ascending branch of the stress-strain curve but the softening behavior of the model shows a steeper curve compared to the test result. Despite the steeper softening data is concentrated at the 45-degree line and only some is scattered away from the equity line. This shows that the curve compared with the test result, the prediction of the residual stress at the end of the stress-strain curve was excellent.

A comparison of the model with specimen N-60-1 tested by Marara, et al. [12] shows the same finding as that between the model with specimen M12 [13]. Comparison of the model with specimen P3 tested by Dhakal, et al. [9] also showed a similar behavior as in the previous comparisons.

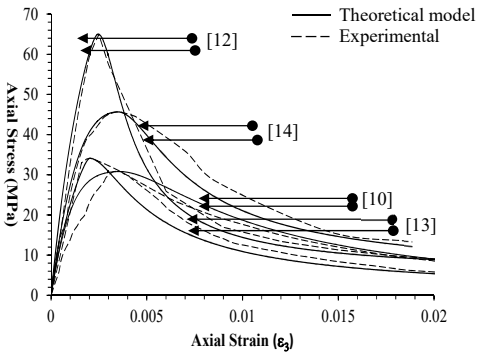

Fig. 4 Comparison of the stress-strain relationship between the selected experimental test and the model [6]

5 The Relationship Between the Ratio of f_r/f'_c and The Ratio of $V_f(l/d)$

This section presents the relationship between the confining pressure level (f_r/f'_c) and the ratio of the fiber volume fraction (V_f) to the fiber aspect ratio (l/d) as

shown in Fig.5. Fig.5, shows an empirical formulation to predict the confining pressure as function of the fiber volume fraction, as well as the fiber aspect ratio. It should be noted that the confining pressure estimates were obtained from the available test results by invoking the equity on the peak stress between the model and the data.

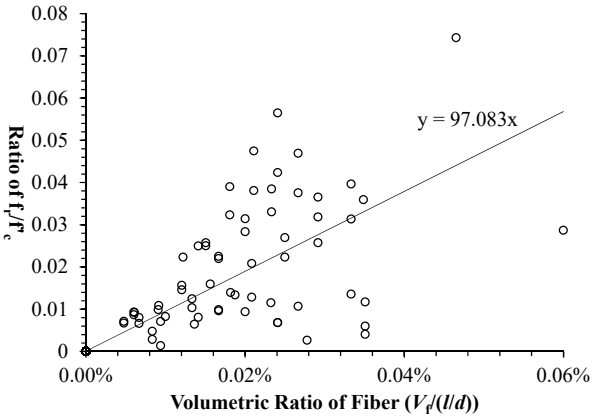

Fig. 5 The confining pressure ratio (f_r/f_c) as function of the ratio of the fiber fraction volume to the fiber aspect ratio ($V_f/(l/d)$)

The expression of the confining pressure level can be estimated as:

$$\frac{f_r}{f_c^{'}} = 0.97\left(\frac{V_f}{l/d}\right) \qquad (4)$$

The formula shown in Eq. (4) will be used in the subsequent analysis of the RC column with and without fiber to get an insight into the behavior of the RC column with steel fiber.

6 Two-Dimensional Nonlinear Sectional Analysis with the Fiber-Based Model

In this section, a two-dimensional nonlinear sectional analysis with fiber-based model is carried out. The analysis is simulated using the computer program code in MATLAB [16]. The RC column is loaded under axial concentric compression. The concrete compressive strength of the RC column is 70 MPa. The column cross-sectional shape is a square column with 400 mm width. The concrete cover is set to 40 mm. The number of longitudinal reinforcing bar used is set to eight with 16 mm diameter. The pitch spacing of the transverse rebar is set to 100 mm. The diameter of the transverse rebar is 10 mm with the total leg number in both x and y direction three, two legs from the close hoops and one leg from the cross tie. The fiber aspect ratio is set to 50 and the fiber volume fractions investigated are 0.00%, 1.00% and 2.00%. Both the longitudinal and the lateral reinforcing bars have a yield strength (f_y) of 400 MPa. The artificial confining pressure provided by the steel fiber is computed using Eq. (4). Fig.6 shows the discretized cross section of the RC column meshed with the constant strain triangle (CST) element.

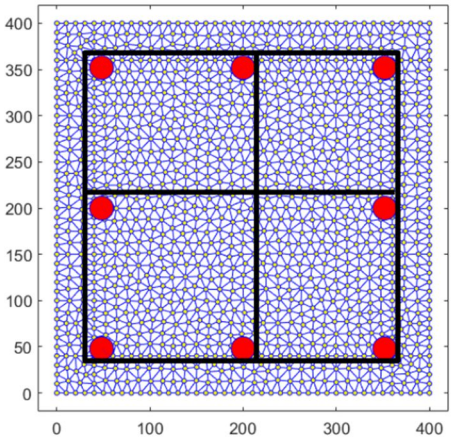

Fig. 6 Discretized cross section of the RC column used in the simulation.

Fig.7 shows the simulation results using the nonlinear fiber-based analysis. For initial tensile confining pressure due to restrained shrinkage [17] was added in the simulation to simulate the behavior of premature cover spalling in high-strength concrete. The ACI 318-14 [18] prediction for squash load was included in the comparison and is:

$$P_o = 0.85 f_c^{'}\left(A_g - A_{st}\right) + f_y A_{st} \qquad (5)$$

where A_{st} is the total area of transverse rebar, A_{st} is the total area of longitudinal reinforcing bar, and A_g is the cross-sectional area of the RC column. It should be noted that the confining rebar of the RC column is not according to the ACI 318-14 specification.

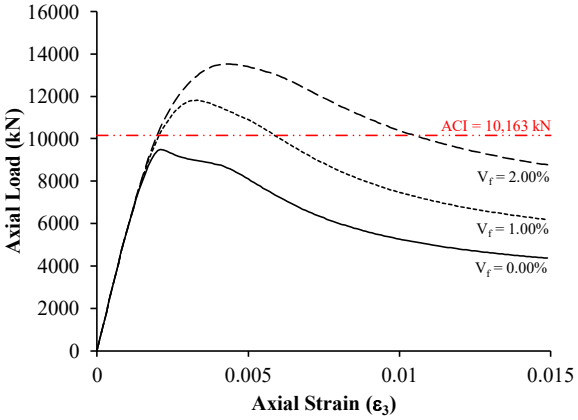

Fig.7 Axial load versus axial strain relationship of the investigated RC column with and without fiber

As shown in Fig.7, from the analysis, the peak load of the column was found below the ACI 318-14 prediction which is not good. With only the addition of 1.00% fiber volume fraction, the peak load of the column is significantly higher than the predicted squash load from ACI 318-14. From the analysis as shown in Fig. 7, the addition of steel fibers about 1.00% and 2.00% fiber volume fraction can increase the peak load of the column by 24,81% and 42,58% compared to the RC column made of plain concrete.

7 Conclusions

This paper investigates the parameter that affects the behavior of concrete when enriched with steel fiber. A method to identify this parameter has been presented. These parameters are the axial peak stress, the residual stress and the axial strain at peak stress. By adjusting the peak stress of the model to the one in the experiments, the confining pressure contributed by the fiber can be computed. Using the computed confining pressure, the predicted residual stress and the axial strain at peak stress can be estimated using any model. In this paper, the Attard and Setunge concrete [6] constitutive model was investigated. The investigation showed that it can be directly used to simulate the behavior of SFRC concrete.

The key parameter was to establish an accurate prediction of the artificial confining pressure contributed by the fiber. For that purpose, a simple formula to estimate the artificial confining pressure has been proposed. However, more experimental data of SFRC under compression is required to validate the proposed expression. In this paper, only the axial direction is considered. In a future study, the lateral direction should be investigated along with the constitutive model in the lateral direction [19, 20].

To gain an insight into the effect of steel fiber in the RC column, a two-dimensional nonlinear sectional analysis has been carried out. The analysis found that the use of steel fiber can improve the strength of the RC column and eliminate the premature cover spalling behavior. In the future, an extension of the analysis from two-dimensional to three-dimensional [21, 22] should be carried out.

References

1. R. P. Dhakal and K. Maekawa, "Reinforcement stability and fracture of cover concrete in reinforced concrete members," *Journal of Structural Engineering,* **128**, no. 10, 1253-1262, (2002).
2. S. J. Foster, "On behavior of high-strength concrete columns: cover spalling, steel fibers, and ductility," *Structural Journal,* **98**, no. 4, 583-589, (2001).
3. S. J. Foster, "The application of steel-fibres as concrete reinforcement in Australia: from material to structure," *Materials and Structures*, **42**, no. 9, 1209, (2009).
4. S. J. Foster, J. Liu, and S. A. Sheikh, "Cover spalling in HSC columns loaded in concentric compression," *Journal of Structural Engineering,* **124**, no. 12, 1431-1437, 1998.
5. S.-C. Lee, J.-H. Oh, and J.-Y. Cho, "Compressive behavior of fiber-reinforced concrete with end-hooked steel fibers," *Materials,* **8**, no. 4, 1442-1458, (2015).
6. M. Attard and S. Setunge, "Stress-strain relationship of confined and unconfined concrete," *ACI Materials Journal,* **93**, no. 5, (1996).
7. B. Piscesa, M. Attard, A. Samani, and S. Tangaramvong, "Plasticity Constitutive Model for Stress-Strain Relationship of Confined Concrete," *ACI Structural Journal,* **114**, no. 2, 361, (2017).
8. A. Samani and M. Attard, "A Stress-Strain Model for Uniaxial and Confined Concrete under Compression," *Engineering Structures,* vol. 41, pp. 335-349, August 2012, doi: http://dx.doi.org/10.1016/j.engstruct.2012.03.027.
9. R. Dhakal, C. Wang, and J. Mander, "Behavior of steel fibre reinforced concrete in compression," (2005).
10. T. Błaszczyński and M. Przybylska-Fałek, "Steel fibre reinforced concrete as a structural material," *Procedia Engineering,* **122**, 282-289, (2015).
11. R. D. Neves and J. F. De Almeida, "Compressive behaviour of steel fibre reinforced concrete," *Structural Concrete,* **6**, no. 1, 1-8, (2005).
12. K. Marara, Ö. Erenb, and İ. Yitmena, "Compression specific toughness of normal strength steel fiber reinforced concrete (NSSFRC) and high strength steel fiber reinforced concrete (HSSFRC)," *Materials Research,* **14**, no. 2, 239-247, (2011).
13. M. Nataraja, N. Dhang, and A. Gupta, "Stress–strain curves for steel-fiber reinforced concrete under compression," *Cement and concrete composites,* **21**, no. 5-6, 383-390, (1999).
14. P. Soroushian and Z. Bayasi, "Fiber type effects on the performance of steel fiber reinforced concrete," *Materials Journal,* **88**, no. 2, 129-134, (1991).
15. D. A. Fanella and A. E. Naaman, "Stress-strain properties of fiber reinforced mortar in compression," in *Journal Proceedings*, **82**, no. 4, 475-483, (1985).
16. B. Piscesa, M. Attard, P. Suprobo, and A. Samani, "Investigation on the fiber based approach to estimate the axial load carrying capacity of the circular concrete filled steel tube (CFST)," in *IOP Conference Series: Materials Science and Engineering*, **267**, no. 1: IOP Publishing, 012017, (2017).
17. B. Piscesa, M. M. Attard, D. Prasetya, and A. K. Samani, "Modeling cover spalling behavior in high strength reinforced concrete columns using a plasticity-fracture model," *Engineering Structures,* **196**, 109336, (2019).
18. A. Committee, and I. O. f. Standardization, "Building code requirements for structural concrete (ACI 318-14) and commentary."
19. B. Piscesa, M. M. Attard, and A. K. Samani, "A lateral strain plasticity model for FRP confined concrete," *Composite Structures,* **158**, 160-174, (2016).
20. A. K. Samani and M. M. Attard, "Lateral Strain Model for Concrete under Compression," *ACI Structural Journal,* **111**, no. 1-6, (2014).
21. B. Piscesa, "Modeling confined concrete using plasticity formulation," PhD. Thesis, School of Civil and Environmental Engineering, The University of New South Wales, Sydney, Australia, (2018).
22. B. Piscesa, M. M. Attard, and A. K. Samani, "3D Finite element modeling of circular reinforced concrete columns confined with FRP using a plasticity based formulation," *Composite Structures,* **194**, 478-493, (2018).